Capturing a mammalian DNA polymerase extending from an oxidized nucleotide

Amy M. Whitaker[†], Mallory R. Smith[†], Matthew A. Schaich and Bret D. Freudenthal[*]

Department of Biochemistry and Molecular Biology, University of Kansas Medical Center, Kansas City, KS 66160, USA

ABSTRACT

The oxidized nucleotide, 8-oxo-7,8-dihydro-2′-deoxyguanosine (8-oxoG), is one of the most abundant DNA lesions. 8-oxoG plays a major role in tumorigenesis and human disease. Biological consequences of 8-oxoG are mediated in part by its insertion into the genome, making it essential to understand how DNA polymerases handle 8-oxoG. Insertion of 8-oxoG is mutagenic when opposite adenine but not when opposite cytosine. However, either result leads to DNA damage at the primer terminus (3′-end) during the succeeding insertion event. Extension from DNA damage at primer termini remains poorly understood. Using kinetics and time-lapse crystallography, we evaluated how a model DNA polymerase, human polymerase β, accommodates 8-oxoG at the primer terminus opposite cytosine and adenine. Notably, extension from the mutagenic base pair is favored over the non-mutagenic base pair. When 8-oxoG is at the primer terminus opposite cytosine, DNA centric changes lead to a clash between O8 of 8-oxoG and the phosphate backbone. Changes in the extension reaction resulting from the altered active site provide evidence for a stabilizing interaction between Arg254 and Asp256 that serves an important role during DNA synthesis reactions. These results provide novel insights into the impact of damage at the primer terminus on genomic stability and DNA synthesis.

INTRODUCTION

Oxidative stress, a cellular condition in which there is an imbalance between concentrations of reactive oxygen species (ROS) and antioxidant defenses, is associated with genomic instability and multiple human diseases (1). ROS can react with nucleotides to generate multiple types of oxidative DNA lesions, both in duplex DNA and the free nucleotide pool. Free deoxynucleotides are even more susceptible to oxidation than duplex DNA (2,3), and incorporation of oxidized nucleotide triphosphates into the genome during replication and repair leads to decreased genomic stability (3–7). Consequently, cells encode an enzyme, human MutT homologue (MTH1), to convert free oxidized nucleotides to their monophosphate form, prohibiting their insertion into the genome (8). Underscoring the significance of the incorporation of oxidized nucleotides into the genome, the inhibition of MTH1 in cancer cell lines promotes cellular death and MTH1 inhibitors are currently in clinical trials (9,10). Given that biological impacts of damaged nucleotides are mediated in part by their insertion and subsequent extension by a DNA polymerase, it is essential to understand how these damaged nucleotides are handled by DNA polymerases at the molecular level (4).

One major oxidized nucleobase resulting from ROS is 8-oxo-7,8-dihydro-2′-deoxyguanosine, which is found in both duplex DNA (8-oxoG) and in the nucleotide pool (8-oxodGTP) (11,12). 8-oxoG arises by the incorporation of an adducted oxygen at C8 and protonation of N7 (13). These modifications to guanine (G) lead to potential mutagenic hydrogen bonding interactions at the Hoogsteen edge (14). The mutagenicity of 8-oxoG is dictated by the *anti-* or *syn-* conformation of the damaged base. Similar to undamaged G, 8-oxoG(*anti*) base pairs with cytosine (C) through classical Watson–Crick hydrogen bonding interactions, forming a non-mutagenic DNA lesion. Alternatively, 8-oxoG(*syn*) is able to exploit its Hoogsteen edge to form a mutagenic base pair with adenine (A). The 8-oxoG:A base pair promotes a G:C to T:A transversion following DNA replication (15). Because of the key role DNA polymerases play in DNA replication and repair, they are important mediators between oxidative stress and the biological outcome of 8-oxoG.

Mammalian DNA polymerase beta (pol β) has been characterized structurally, kinetically, and biologically (16,17). Consequently, pol β has served as a model enzyme for characterizing the nucleotidyl transferase reaction, which is utilized universally by DNA polymerases during DNA synthesis. Pol β is employed during DNA repair as

---

[*]To whom correspondence should be addressed. Tel: +1 913 588 5560; Fax: +1 913 588 9896; Email: bfreudenthal@kumc.edu
[†]These authors contributed equally to this work as first authors.

part of the base excision repair pathway (BER), where it primarily preforms gap filling DNA synthesis during single nucleotide replacements. In a long-patch variation of the BER pathway, pol β has also demonstrated the ability to fill gaps 2–6 nucleotides in length. The polymerase domain of pol β, analogous to other DNA polymerases, is composed of three functionally distinct subdomains. Pol β binds to gapped DNA substrates in the open conformation using its DNA binding- or D-subdomain. This binary complex (pol β/DNA) positions the templating base and primer terminus within the active site. A conformational change from an open to closed state occurs at the nascent base pair binding domain (N-subdomain) upon binding of the incoming nucleotide. In the closed conformation, pol β repositions the 3′-OH of the deoxyribose at the primer terminus for in-line attack on the α-phosphate (Pα) of the incoming dNTP. In this state, the catalytic subdomain (C-domain) of pol β coordinates two divalent metal cations that facilitate DNA synthesis. Upon catalysis, pyrophosphate (PPi) is formed and released when pol β re-opens.

Employing pol β as a model DNA polymerase, structural changes within the active site, emanating from substrates containing 8-oxoG in the templating strand ([18],[19]) or the insertion of 8-oxodGTP, have led to mechanistic insights ([4]). These crystallographic studies have demonstrated that a clash, between the adducted oxygen (O8) and the phosphate backbone of 8-oxoG, can promote antagonistic changes to the nucleoside sugar pucker and backbone position. Additionally, insertion of 8-oxodGTP leads to overall instability at the newly generated primer terminus. During the subsequent round of DNA synthesis, the polymerase is tasked with extending from the 8-oxoG terminated primer strand. Unfortunately, very little is known about how polymerases extend from a damaged primer terminus. In this study, we utilized kinetics and time-lapse X-ray crystallography to decipher the impact of 8-oxoG at primer termini during DNA synthesis. These studies revealed mutagenic extension from 8-oxoG:A is substantially favored in comparison to the non-mutagenic pairing of 8-oxoG:C. Reduced extension proficiency with non-mutagenic 8-oxoG:C primer termini arises from active site rearrangements accommodating O8 of 8-oxoG in a base pair dependent fashion.

MATERIALS AND METHODS

DNA sequences

The following DNA sequences were used to generate the 16-mer DNA duplexes used in crystallization studies (the nucleotide opposite 8-oxoG is underlined): template, 5′-CCGACG(C/A)CGCATCAGC-3′; primer, 5′-GCTGATGCG-3′; downstream, 5′-GTCGC-3′. The downstream sequence was 5′-phosphorylated. The kinetic studies required extending the downstream and upstream sequences to employ a 34-base DNA substrate. The sequence of the template strand was 5′-GTACCCGGGGATCCGT ACG(C/A)CGCATCAGCTGCAG-3′. DNA substrates for single-nucleotide gap filling DNA synthesis reactions were prepared by annealing three purified oligonucleotides. Each oligonucleotide was suspended in 10 mM Tris–HCl, pH 7.4 and 1 mM EDTA and the concentration was determined from their ultraviolet absorbance at 260 nm. The annealing

reactions were performed by incubating a solution of primer with downstream and template oligonucleotides (1:1.2:1.2 molar ratio, respectively) at 95°C for 5 min, followed by 65°C for 30 min, and finally cooling 1°C min^{-1} to 10°C in a thermocycler.

Expression and purification of pol β

Human wild-type DNA pol β was overexpressed from a pET-30 vector in the BL21-CodonPlus(DE3)-RP *Escherichia coli* strain. Purification of pol β was carried out as described previously and briefly written here ([20]). Cell lysate containing pol β was run over GE HiTrap Heparin HP, GE Resource S, and HiPrep 16/60 Sephacryl S-200 HR columns and fractions containing pure pol β were concentrated and stored at –80°C in 20 mM BisTris propane, pH 7.0 for crystallization and 50 mM HEPES, pH 7.4 for kinetics. Pol β was determined to be pure by SDS page and the final concentration was determined by A_{280} using a NanoDrop One UV-Vis Spectrophotometer (ϵ = 23 380 M^{-1} cm^{-1}).

Pol β steady-state kinetic characterization

The steady-state kinetic parameters for the extension from 8-oxoG by pol β were determined by performing initial velocity measurements of a single-nucleotide gap filling reaction as previously described ([28]). DNA substrates contained a 5′,6-carboxyfluorescein and were designed with an 8-oxoG or non-damaged G at the 3′-terminus base paired with C or A. The reaction mixture used to obtain activity measurements contained 50 mM Tris–HCl, pH 7.4 (37°C), 100 mM KCl, 10 mM MgCl$_2$, 1 mM dithiothreitol, 100 μg/ml bovine serum albumin, 10% glycerol and 200 nM single-nucleotide gapped DNA. 50 μl reactions were stopped by addition of an equal volume of a quenching solution containing 100 mM EDTA, 80% deionized formamide, 0.25 mg/ml bromophenol blue and 0.25 mg/ml xylene cyanol. Enzyme concentrations and reaction times were selected to maintain initial velocity conditions. Product and substrate DNA were separated on a 16% denaturing (8 M urea) polyacrylamide gel. The resulting bands were quantified using a GE Typhoon 8600 imager in fluorescence mode using a 532 nm excitation laser and 526 nm short-pass emission filter. Steady-state kinetic parameters (K_M, k_{cat}) were determined by fitting the data to the Michaelis–Menten equation. The relative extension efficiency, f_{ex}, was calculated from the ratio of catalytic efficiencies for correct dCTP insertion on a matched, non-damaged (G–C) and modified primer terminus. The mean and standard error of at least three independent experiments are shown on the graphs in Figure [1].

Crystallization of pol β

Pol β was initially complexed with 2-nt gapped DNA and incubated with 8-oxodGTP. This incubation resulted in a 1-nt gap DNA substrate with 8-oxoG at the primer terminus inserted across from either A or C. Binary complex crystals with 8-oxoG:A or 8-oxoG:C at the primer terminus were grown as previously described in a solution containing 50 mM imidazole, pH 7.5, 13–19% PEG3350 and

350 mM sodium acetate (21). In order to visualize multiple enzymatic states, time-lapse crystallography was utilized as previously described and summarized here (18). First, binary pol β/DNA crystals were soaked in a cryosolution containing 25% ethylene glycol, 50 mM imidazole, pH 7.5, 19% PEG3350 and 70 mM sodium acetate, 2 mM dCTP and 50 mM CaCl$_2$ for 20 min. These ground state ternary pol β/DNA/dNTP crystals were subsequently transferred to a cryosolution containing 25% ethylene glycol, 50 mM imidazole, pH 7.5, 19% PEG3350, 70 mM sodium acetate, and 200 mM MgCl$_2$ or MnCl$_2$ for the varying, indicated times.

Data collection and refinement

Data were collected at 100 K on a Rigaku MicroMax-007 HF rotating anode diffractometer equipped with a Dectris Pilatus3R 200K-A detector system at a wavelength of 1.54 Å. Data were processed and scaled using the HKL3000R software package (22). Initial models were determined using molecular replacement with the previously determined open (PDB: 3ISB), closed (PDB: 2FMS), or mismatch (PDB: 3C2M) structures of pol β as a reference. All R-free flags were taken from the starting model. Refinement was performed using PHENIX and model building using Coot (23,24). The metal ligand coordination restraints were generated by ReadySet (PHENIX). Partial catalysis models were generated with both the reactant and product species, and occupancy refinement was performed. The figures were prepared in PyMOL (Schrödinger LLC). Ramachandran analysis determined 100% of non-glycine residues lie in the allowed regions and at least 98% in favored regions.

RESULTS

Kinetic characterization of extension from 8-oxoG

The ability of a DNA polymerase to extend from 8-oxoG at primer termini was evaluated using pol β and steady-state kinetic analysis. This approach utilized a 1-nt gapped DNA substrate with a templating G and either 8-oxoG:C, 8-oxoG:A, G:C or G:A at the primer terminus. This array of substrates allowed for a thorough comparison of extension from non-damaged and damaged primer termini. Results are summarized in Figure 1 and kinetic parameters are listed in Supplementary Table S1. The apparent affinity of an incoming dCTP to pol β with a 1-nt gapped DNA substrate (K_M) with each 3′-terminus combination was determined. The presence of 8-oxoG at the primer terminus, in the form of either an 8-oxoG:A or 8-oxoG:C base pair, resulted in similar K_M values for the incoming dCTP of 0.3 and 0.2 μM, respectively (Figure 1A, Supplementary Table S1). These apparent binding affinities are comparable to what was obtained for dCTP to the pol β/DNA complex with a matched, non-damaged G:C base pair at the primer terminus ($K_M = 0.09$ μM), but in contrast to a G:A ($K_M = 24$ μM). On the other hand, enzymatic turnover rates (k_{cat}) are considerably different depending on which base is across from 3′-8-oxoG, with C and A producing rates of 0.017 and 0.30 s^{-1}, respectively (Figure 1B, Supplementary Table S1). In comparison, the rate of enzymatic turnover for the non-damaged, mismatched G:A is 0.092 s^{-1}, while matched G:C
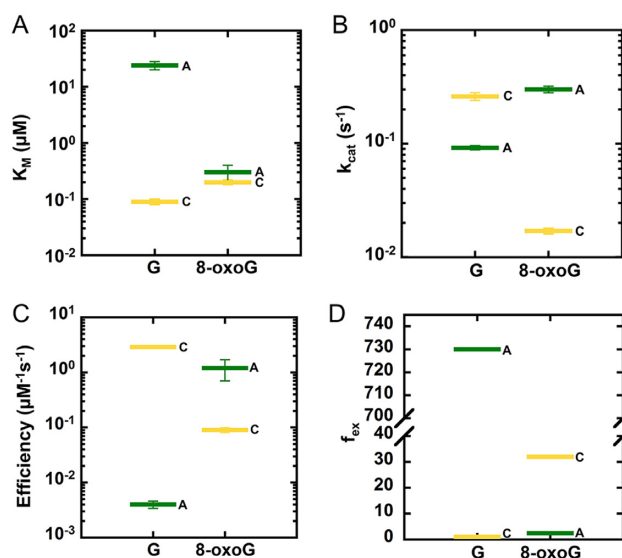

Figure 1. Kinetic characterization of extension from 8-oxoG by pol β. (**A**) K_M, (**B**) k_{cat} and (**C**) catalytic efficiencies pol β dCTP insertion opposite G with substrates containing either dGTP or 8-oxodGTP at the primer terminus opposite C and A. (**D**) f_{ex} values corresponding to (C). Green bars represent A, and yellow represents C. The results represent the mean (SE) of at least three independent determinations. The identity of the primer terminus is given as primer nucleotide/template nucleotide.

is 0.26 s^{-1}. This turnover rate for a non-damaged, matched terminus is nearly identical to 8-oxoG:A, in contrast to extension from 8-oxoG:C which is ∼15-fold slower. The resulting catalytic efficiencies, k_{cat}/K_M, are 0.09 μM^{-1} s^{-1} (8-oxoG:C) and 1.2 μM^{-1} s^{-1} (8-oxoG:A), compared to 2.9 and 0.0040 μM^{-1} s^{-1} for non-damaged G:C and G:A, respectively (Figure 1C, Supplementary Table S1).

To provide a rational method for comparing the differences in catalytic efficiency between the matched, non-damaged G:C primer terminus and either mismatched (G:A) or 8-oxoG containing termini, we have also reported relative extension efficiency (f_{ex}) values (Figure 1D, Supplementary Table S1) (19). For each 3′-terminus, the f_{ex} value represents the fold change in catalytic efficiency between the substrate with the terminus of interest and the substrate with a G:C terminus. Hence, f_{ex} describes the efficiency of extension relative to that from the matched, non-damaged primer terminus, where values >1 correspond to termini with reduced extension efficiencies and larger magnitudes represent reduced efficiency. Experimental f_{ex} values for 8-oxoG:A and 8-oxoG:C are 2.3 and 32, respectively. This large reduction in relative extension efficiency observed with 8-oxoG at the primer terminus opposite C, but not A, implies 8-oxoG alters the active site differently depending on its base-pairing partner. Furthermore, the measured differences in catalytic efficiency between the two damaged termini stem from variation in the enzymatic turnover rates, as demonstrated by differences in k_{cat}, as opposed to their comparative apparent nucleotide binding affinities (K_M). Additionally, extension efficiencies vary greatly between the damaged mismatch 8-oxoG:A ($f_{ex} = 2.3$) and the non-damaged mismatch G:A ($f_{ex} = 730$). This is presumably from the reduced apparent affinity for substrate, demon-
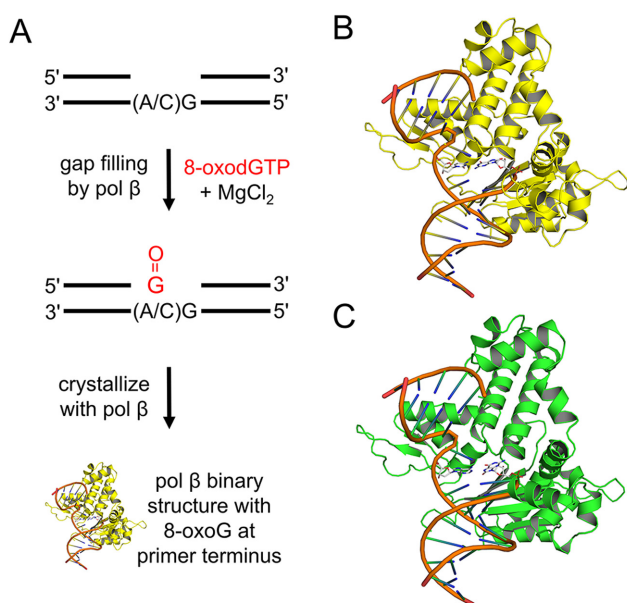
Figure 2. Construction of 8-oxoG terminated pol β DNA substrates. (**A**) Schematic demonstrating pol β insertion of 8-oxodGTP (red) to generate substrates for subsequent crystallization with 8-oxoG opposite A and C at the primer terminus. (**B**) Binary structure showing 8-oxoG at the primer terminus opposite C (yellow). (**C**) Binary structure showing 8-oxoG opposite A at the primer terminus (green). The primer terminal base pairs are shown as sticks in gray.

strated by the 80-fold larger K_M with G:A at the primer terminus, indicating O8 of 8-oxoG promotes a primer terminus conformation suitable for nucleotide binding. Because pol β binds DNA in an open conformation, we do not expect 8-oxoG at the primer terminus to alter the affinity of pol β for single-nucleotide gapped DNA. Additionally, it has previously been shown that mismatched primer termini do not affect single-nucleotide gapped DNA binding affinity for pol β (25,26).

Binary complex structures with 8-oxoG at the primer terminus

To gain molecular insight into the impact an 8-oxoG terminated primer has on the polymerase active site, we employed X-ray crystallography of pol β. To generate 1-nt gapped DNA substrates with 8-oxoG at the primer terminus, we utilized pol β polymerase activity prior to crystallization (Figure 2A). Pol β was incubated with 8-oxodGTP and a 2-nt gapped DNA substrate containing C or A followed by G in the gap, resulting in 8-oxoG incorporation opposite either C or A at the primer terminus with a G in the 1-nt gap. This protein/DNA mixture was subsequently used during crystallization to form binary pol β/DNA complexes with either an 8-oxoG:C or 8-oxoG:A base pair at the primer terminus. Our binary pol β structures, described below, confirmed that 8-oxoG was inserted at the primer terminus adjacent to a 1-nt gap containing a G (Figure 2B and C).

Binary X-ray crystal structures show pol β in its open conformation while bound to 1-nt gapped DNA with 8-oxoG at the primer terminus opposite either C or A at 1.80 and 1.95 Å resolution, respectively (Supplementary Table
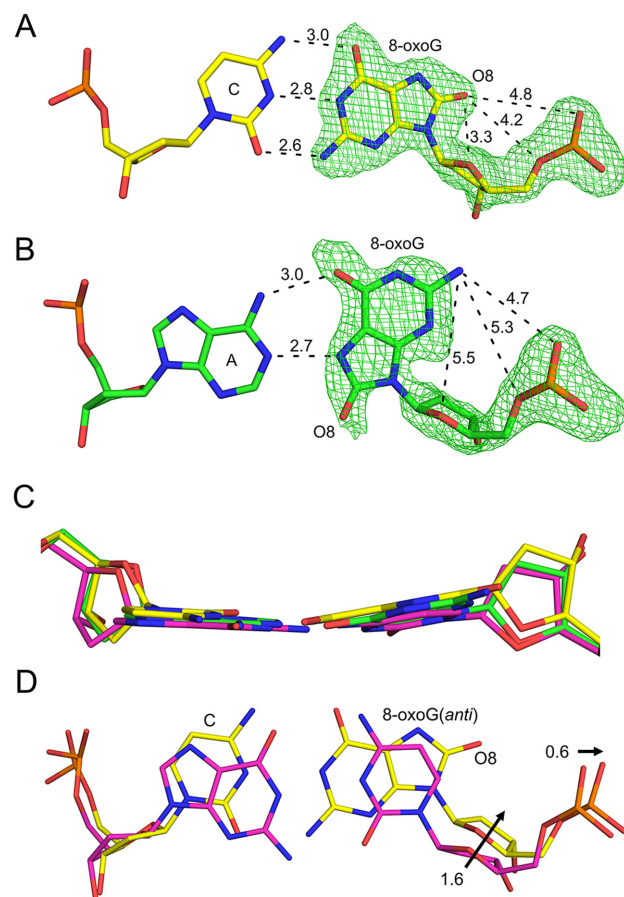

Figure 3. Binary complex structures with 8-oxoG at the primer terminus. (**A**) Primer terminus 8-oxoG:C Watson–Crick base pair (yellow). (**B**) Primer terminus 8-oxoG:A Hoogsteen base pair (green). (**C**) A 90° rotation demonstrates planarity of 8-oxoG containing base pairs overlaid with non-damaged, matched binary reference structure (magenta, PDB 3ISB). (**D**) In reference to 3ISB (magenta), a primer terminus 8-oxoG:C (yellow) results in shifts (arrows) in the sugar and Pα of 8-oxoG(*anti*). The omit maps (green) are contoured at 3σ. Distances are labeled and indicated as dashed lines.

S2). These structures provide insight into how 8-oxoG is situated at primer termini in the binary state prior to nucleotide binding. When 8-oxoG is opposite either A or C, it forms an ordered and stable primer terminus as indicated by clear density and a low B-factor (Supplementary Tables S2 and S3, Figure 3A and B). This stability is achieved by hydrogen bonding interactions between 8-oxoG and the opposing base. 8-oxoG(*anti*) hydrogen bonds with C using its canonical Watson-Crick face (Figure 3A) and to A in the *syn*-conformation using its Hoogsteen face (Figure 3B). Both 8-oxoG containing base pairs sit planar at the primer terminus and there is no significant repositioning compared to non-damaged, correctly paired DNA (i.e. G:C) (Figure 3C). The sugar pucker of 8-oxoG at the primer terminus is O4′-endo while paired with either A or C, which contrasts to binary non-damaged, matched primer termini that adopt C4′-exo at the primer terminus (PDB 3ISB). In addition to the sugar pucker change, when 8-oxoG(*anti*) is opposite C the nucleoside shifts by 1.6 Å toward the ma-

jor groove (Figure 3D). This movement may arise from the phosphate backbone shifting 0.6 Å away from O8 when 8-oxoG is in the *anti*-conformation. When 8-oxoG is in the *syn*-conformation, O8 of 8-oxoG is in the minor groove of the DNA, which prevents clashing with active site residues.

8-oxoG opposite C breaks the Arg254 and Asp256 salt bridge

To obtain ternary pol β complexes, we started with binary pol β/DNA complexes with 8-oxoG:C at the primer terminus generated as described above. These crystals were transferred to a cryoprotectant solution containing Ca^{2+}, which does not support catalysis, and dCTP to promote the formation of the closed pre-catalytic ternary pol β complex. The crystal diffracted to 2.2 Å, Supplementary Table S2. Figure 4A shows a close-up of the active site with the dCTP bound, Ca^{2+} in the nucleotide (Me_n) and catalytic (Me_c) metal binding sites, and 8-oxoG:C at the primer terminus. The metal ions and incoming dCTP adopt a nearly identical conformation as observed with a non-damaged, matched primer terminus (Supplementary Figure S1). The only major structural changes are localized around the 8-oxoG:C primer terminus base pair.

Upon binding dCTP, the sugar pucker of 8-oxoG shifts from O4′-endo to C3′-endo, likely as a result of the 8-oxoG 3′-OH coordinating Ca^{2+} in the Me_c site. 8-oxoG maintains the *anti*-conformation and planar Watson–Crick hydrogen bonding interactions with C. In this conformation, the clash between O8 and the phosphate backbone forces a 1.7 Å shift of the backbone away from O8. This shift leads to a 110° rotation and 5.5–6 Å displacement of Arg254 in the pol β active site (Figure 4B), causing a disruption of the salt bridge between Arg254 and Asp256 (Figure 4C) that is postulated to stabilize Asp256 in pol β structures with non-damaged primer termini (see discussion) (27). To ensure the rotation of Arg254 was not Ca^{2+} dependent, a higher resolution structure was obtained after a soak in the biological polymerase co-factor Mg^{2+} and a non-hydrolysable nucleotide analog, 2′-deoxycytidine-5′-[(α,β)-methyleno]triphosphate (dCpCpp), to prevent the catalysis. The 2.0 Å resolution structure confirmed metal independence (Figure 4D).

Watching extension from 8-oxoG:C by time-lapse crystallography

Both the kinetic binding constant (K_M) and ternary ground state structure (Supplementary Table S1 and Figure 4) indicate that pol β can accommodate dCTP binding easily with an 8-oxoG at the primer terminus opposite C. The active site residue Arg254 shifts out of the catalytically optimal orientation, however the mechanism of extension is indecipherable from the pre-catalytic structure alone. In order to understand how 8-oxoG:C alters catalytic efficiency, we utilized time-lapse X-ray crystallography to look at structural changes at the molecular level over the course of catalysis. This approach captures reactant state structures undergoing nucleotidyl transfer by first generating crystals of ternary complexes (pol β/DNA/dCTP) in the presence of the inert metal Ca^{2+} before initiating the reaction by soaking the crystal in a solution of $MgCl_2$ (18). The reaction is
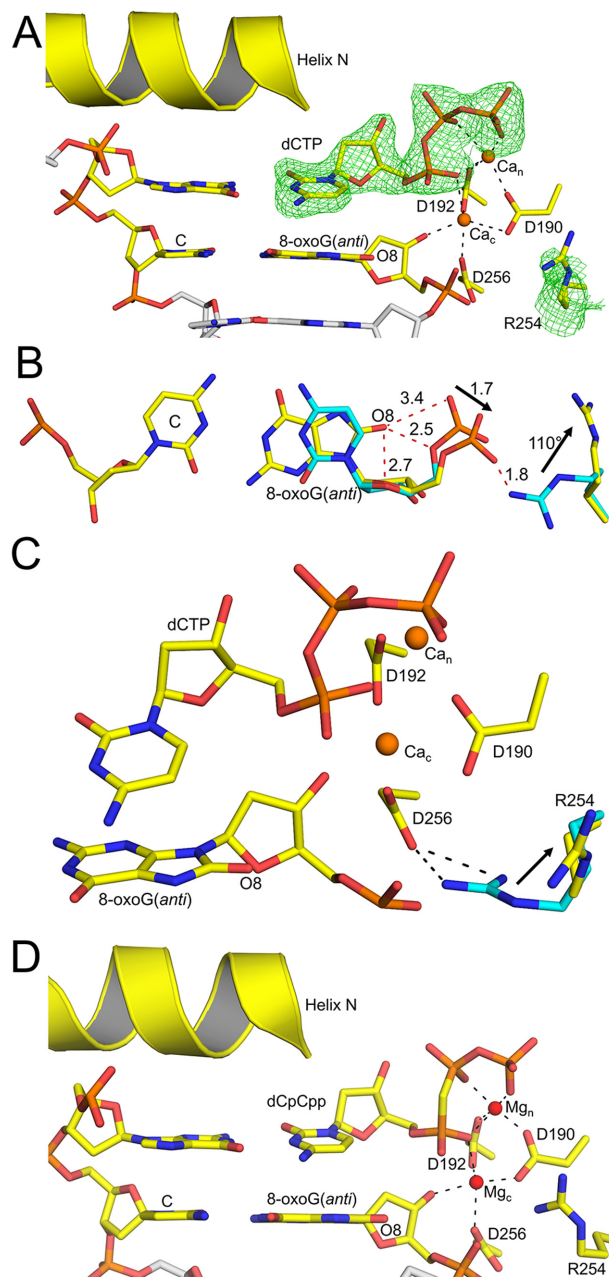

Figure 4. Ternary ground state structures with 8-oxoG:C at the primer terminus. (**A**) Pre-catalytic complex with dCTP and inert Ca^{2+} bound. (**B**) A 90° rotation relative to (A). Clashing at O8 and Pα is shown as red dashes and shifts are indicated with arrows in reference to a non-damaged primer terminus (cyan, PDB 2FMS). (**C**) Close-up of the active site demonstrating the loss of the salt bridge interaction between Asp256 and Arg254 (shown with 2FMS, cyan) when 8-oxoG:C is at the primer terminus (yellow). (**D**) Pre-catalytic complex with non-hydrolysable analog, dCpCpp, and catalytic metal, Mg^{2+}, bound. The omit map (green) is contoured at 3σ. H-bonds are shown as black dashed lines, and clashes are shown as red dashed lines. Ca^{2+} and Mg^{2+} are orange and red spheres, respectively.

subsequently stopped in a time dependent fashion by flash freezing, followed by structure determination of the crystal. A structure with 8-oxoG:C at the primer terminus was collected after a 60 s soak in $MgCl_2$ that diffracted to 2.08 Å. Density corresponding to both the reactant and prod-
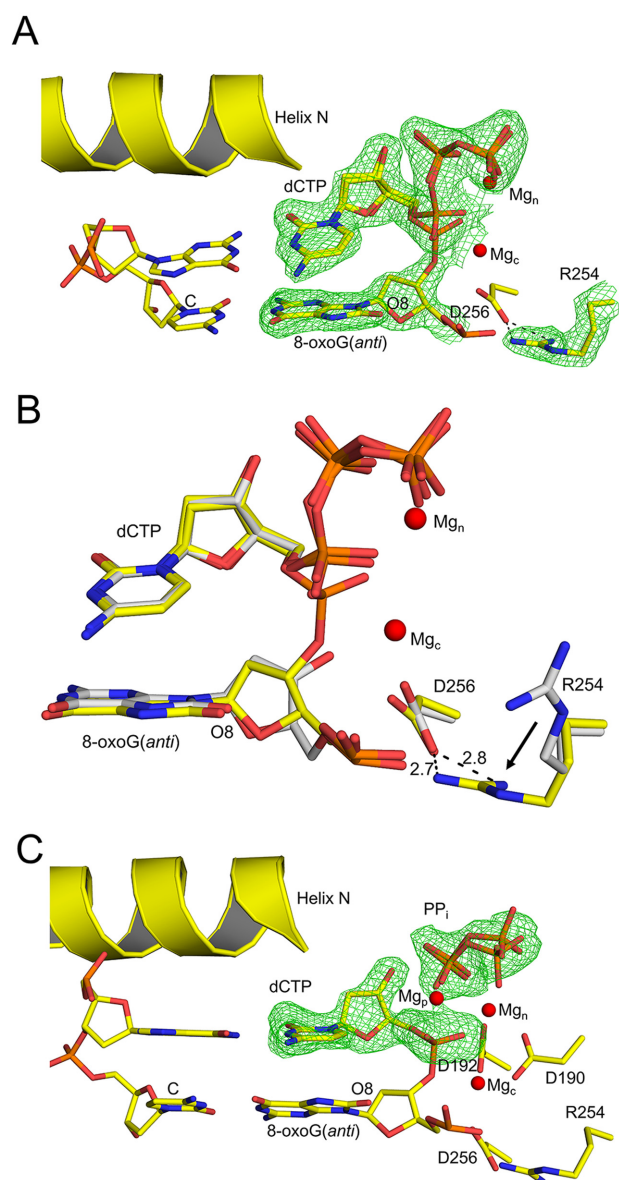
Figure 5. Pol β extension from 8-oxoG:C by time-lapse X-ray crystallography. (**A**) The active site after a 60 s soak in MgCl$_2$. (**B**) An overlay of the reactant state (yellow) and the ground state (gray) active sites demonstrating the swing of Arg254 back into the catalytically competent position. (**C**) The closed, completed product active site after a 120 s soak in MgCl$_2$. The omit maps (green) are contoured at 3σ. Red spheres are Mg^{2+}. H-bonds are shown as black dashed lines.

To observe the product complex with 8-oxoG:C at the primer terminus, we utilized the same approach, but extended our MgCl$_2$ soak time to 120 s prior to collecting the 2.05 Å resolution product structure (Supplementary Table S2). At this point, the synthesis reaction was complete, shown by insertion of dCMP and formation of pyrophosphate (Figure 5C). The sugar pucker of 8-oxoG maintains C3′-endo. In this product complex, Arg254 remains in a stable salt bridge with Asp256. As shown in previous pol β product structures, a third product associated metal ion is present (4,18,28). In this product complex, the polymerase remains in the closed conformation. It has previously been shown that the closed to open conformational cha411nge of pol β following insertion is altered depending on the identity of the nucleotide (i.e. matched, mismatched, damaged) (4,18). To establish whether 8-oxoG promotes re-opening of the polymerase *in crystallo*, we extended the time of our soak in MgCl$_2$. This resulted in pol β undergoing the closed to open transition accompanied by a loss of hydrogen-bonding interactions between the inserted dCMP and templating G while 8-oxoG remained base paired to C (Supplementary Figure S2).

8-oxoG:A at the primer terminus is poised for catalysis upon metal binding

To determine the molecular structure of 8-oxoG:A at the primer terminus, we soaked a binary 8-oxoG:A pol β crystal in a cryoprotectant solution with CaCl$_2$ and dCTP. The resultant closed ternary ground state crystal diffracted to 2.1 Å. This structure has an incoming dCTP base pairing with a templating G and the primer terminal 8-oxoG in the *syn*-conformation hydrogen bonding to A through its Hoogsteen face (Figure 6A). The sugar pucker changes to C2′-endo in the ground state, a conformation that has been demonstrated to inhibit insertion (29). This is altered from the 8-oxoG:C pre-catalytic structures which shifted into the catalytically optimized C3′-endo upon nucleotide binding. In this conformation, the N2 of 8-oxoG*(syn)* hydrogen bonds to the non-bridging oxygen of the phosphate backbone, and Arg254 maintains the salt bridge with Asp256 (Figure 6B and C). In addition, Tyr271 is within hydrogen bonding distance of O8 (Figure 6C). These favorable interactions contrast the unfavorable interactions between the phosphate backbone and O8 with 8-oxoG in the *anti*-conformation (Figure 4B).

A close-up of the active site in Figure 6B shows 8-oxoG:A at the primer terminus with Ca^{2+} bound in the Me$_n$ site and a water molecule in the Me$_c$ site. The lack of a metal in the Me$_c$ site results in the 3′-OH shifting to a non-catalytic conformation that does not support in-line nucleophilic attack. The distance between the 3′-OH and the Pα is 4.2 Å, as opposed to 3.4 Å, which is optimized for catalysis in the reference structure (PDB 2FMS). Similarly, when the ternary complex was crystallized with the non-hydrolysable analog, dCpCpp, in the presence of MgCl$_2$, a water molecule is in the Me$_c$ site, and the 3′-OH is shifted (Supplementary Figure S3). This suggests that even though Me^{2+} does bind at the catalytic metal site (see product structures below), the Me^{2+} binding is less efficient than when C is at the template-primer terminus across 8-oxoG. This is indicated by the cor-

uct states was observed (Figure 5A), indicating the reaction was 20% complete. Figure 5B shows a comparison of this reactant structure with the ground state. Upon initiation of catalysis, Arg254 realigns into a catalytically competent position where it coordinates Asp256 (Figure 5B), as observed for the non-damaged primer terminus (PDB: 2FMS). Thus, indicating Arg254 must first swing back to coordinate Asp256 for catalysis, providing a structural basis for the reduced k_{cat} observed in the steady-state kinetic analysis (Figure 1 and Supplementary Table S1).
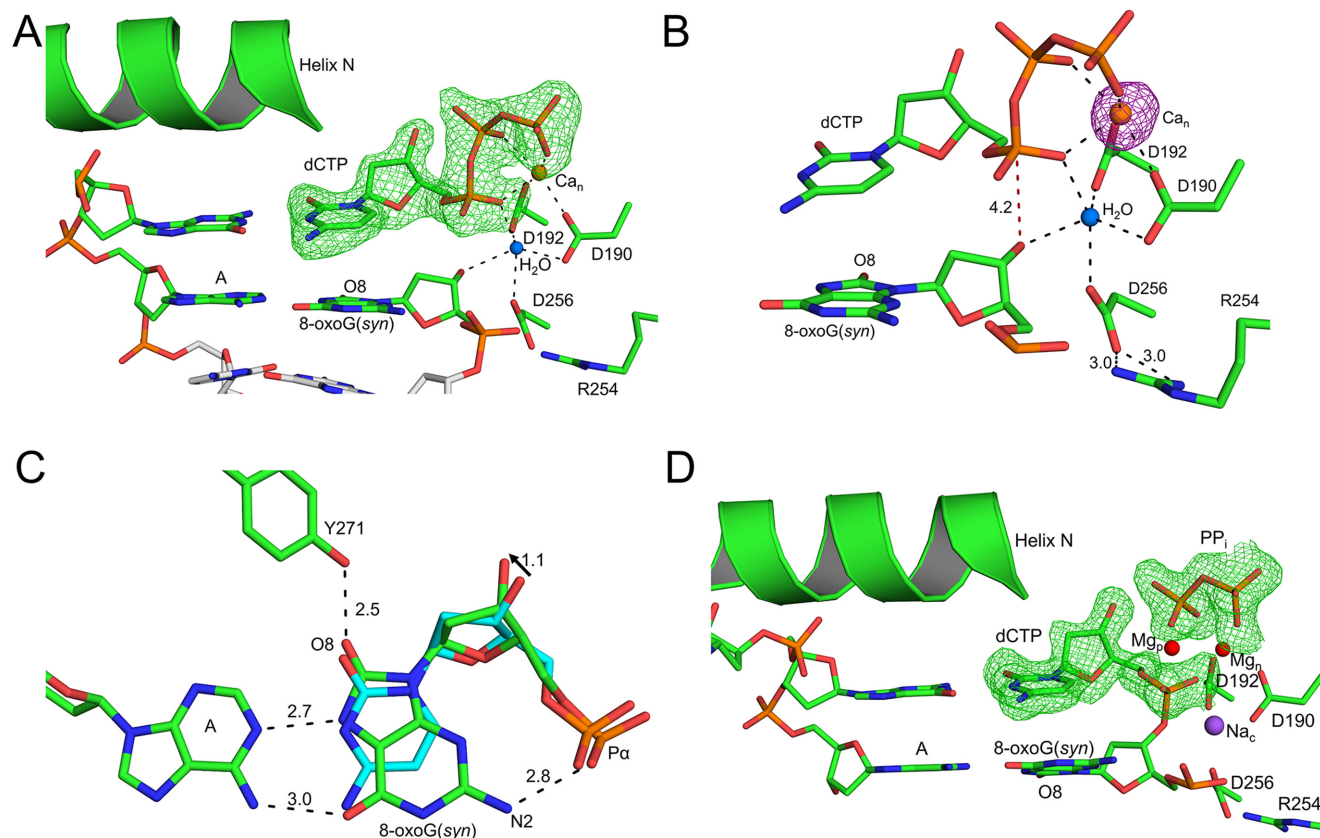
Figure 6. Ternary ground state structures with 8-oxoG:A at the primer terminus. (**A**) Pre-catalytic complex with dCTP, Ca^{2+} in Me_n and water in Me_c bound. (**B**) A close-up of the active site. Interaction between Asp256 and Arg254 is maintained. Distance between 3'-OH and $P\alpha$ of dCTP is shown as a red dashed line. (**C**) Stabilizing interactions are shown at the terminal base pair. Shift in 3'-OH is indicated by an arrow. (**D**) The closed, completed product active site after a 20 s soak in $MgCl_2$. Ca^{2+}, Mg^{2+}, Na^{2+} and H_2O are orange, red, purple, and blue spheres, respectively. Magenta is an anomalous map contoured at 4σ. H-bonds are shown as black dashed lines.

responding ternary structure with C, which has Ca^{2+} ions bound in both metal sites. When interpreted in the context of the catalytic efficiencies, it appears additional stabilizing features at the primer terminus between Tyr271 and O8, and N2 with the phosphate backbone compensate for the weakened Me^{2+} binding at the catalytic metal site.

Attempts to observe catalysis by soaking ground state crystals in a solution containing $MgCl_2$ failed to produce reactant state structures that contain a mixture of both substrate and product. We either obtained structures that were in the ground state (dCTP bound) or had been converted to all product (dCMP inserted). One possibility for the difficulty in capturing a reactant state is that the Mg^{2+} ion can quickly bind to the Me_c site to initiate catalysis, which is in contrast to other time-lapse structures with a Ca^{2+} in the Me_c that must exchange prior to catalysis occurring. Therefore, the reaction likely undergoes catalysis faster than we can capture using a manual approach. The resulting product structure was obtained at a resolution of 1.8 Å with Mg^{2+} bound at the Me_n site, and Na^{2+} bound at the Me_c site. This structure indicates as soon as Mg^{2+} binds to the Me_c site, catalysis occurs with minimal changes between the ground and product state structures (Figure 6D and Supplementary Table S3). After catalysis has occurred, the Mg_c ex-

changes for Na_c (18). The only major change is the appearance of a third metal ion upon complete product formation that is consistent with previous early product structures observing catalysis *in crystallo* (18). Of note, 8-oxoG remains in the *syn*-conformation with potential hydrogen bonding interactions between Tyr271 and O8, and N2 and the phosphate backbone oxygen. The only structural change observed upon catalysis, which occurs upon nucleotide binding with 8-oxoG:C, is a shift in the sugar pucker to C3'-endo. As was previously observed for correct insertion of dCTP across from G with a non-damaged substrate, pol β with the 8-oxoG:A base pair remained in a closed conformation after an extended soak, in contrast to the 8-oxoG:C structure. Overall, the ground state and product structures obtained with A across from the primer terminus indicate minimal structural rearrangements are required for catalysis.

DISCUSSION

Insertion of a modified nucleotide by a DNA polymerase results in DNA damage positioned at the primer terminus, which will be the substrate during subsequent rounds of DNA synthesis. The oxidized purine 8-oxoG, generated by oxidative stress, is the most abundant of the various modi-

fied DNA bases and plays a major role in mutagenesis and tumorigenesis. Using kinetics and time-lapse X-ray crystallography, we have evaluated how pol β accommodates 8-oxoG at the primer terminus and revealed the molecular contacts involved during extension from both mutagenic and non-mutagenic 8-oxoG base pairs (Figure 7).

Pol β accommodates the mutagenic 8-oxoG:A base pair at the primer terminus

Our open binary complex structures demonstrate that 8-oxoG(*syn*) across from A at the primer terminus forms a stable (25.6 Å^2) Hoogsteen base pair in the absence of an incoming dNTP. This contrasts what was seen in previous reported structures characterizing the insertion of 8-oxoG(*syn*) across from A, where a high B-factor (57 Å^2) and a loss of hydrogen bonding between the bases was observed at the new primer terminus in the post-catalysis open product complex (17). Of note, in this product structure, the primer terminus is not in the correct registry for insertion of the next nucleotide, as it is in the structures reported here, suggesting that active site contacts stabilize 8-oxoG(*syn*) at the primer terminus when in the proper registry. Once the nucleotide is bound and the enzyme shifts into the closed conformation, the only repositioning required for catalysis to occur is a change in the sugar pucker, and the binding of the catalytic metal. The lack of substantial structural rearrangements required for extension from a mutagenic 8-oxoG:A base pair is supported by the high catalytic efficiency. Additionally, our structures showed the damage, O8, is accommodated at the primer terminus by being positioned in the minor groove of the DNA. Similarly, accurate replication beyond a bulky major benzo[a]pyrene adduct by human DNA polymerase kappa was shown to be accomplished by positioning the damage in the nascent DNA minor groove (30).

Because the biological outcomes of 8-oxoG are mediated in part by the perturbations to the DNA synthesis reaction provoked by the modified structure of the lesion, it is important to have a thorough understanding of how DNA polymerases respond to the damage. Accordingly, previous studies have determined the effects of 8-oxoG on the mechanism of model mammalian DNA polymerase, pol β, both structurally and kinetically, with the damage in the templating position, the template strand primer terminus (*n* – 1), and as the incoming nucleotide (4,19,31,32). While the catalytic efficiencies are similar to that with a non-damaged substrate, the strategies employed by pol β to accommodate 8-oxoG(*syn*) adapt, depending upon which registry contains the damage. Insertion of 8-oxodGTP*(syn)* across from A relies on interactions between Pα and N2 of 8-oxoG(*syn*) and active site residue Asn279 with O8 (4). In the case of a templating 8-oxoG, the transition to the *syn*-conformation with an incoming dATP requires contacts between 8-oxoG(*syn*) and residue Arg283, which is a key minor groove contact in the pol β active site (84). The template strand has a 90° bend at the position of the templating base, resulting in an absence of protein interactions and intrinsic flexibility of the phosphodiester backbone. This flexibility allows for a 3.4 Å shift in the phosphate backbone of 8-oxoG in the template position. No shift of the phosphodi-

ester backbone is observed when the 8-oxoG(*syn*):A base pair is at the template primer terminus (*n* – 1) (19). Overall, the different strategies indicate a registry dependent processing of 8-oxoG within the pol β active site, emphasizing the importance of characterizing each of these positions.

8-oxoG:C results in a clash at the phosphate backbone

Our binary structure shows stable (B-factor = 24.9 Å^2) Watson–Crick hydrogen bonds between 8-oxoG(*anti*) and C at the primer terminus. As also recognized in the mutagenic case with A, previously reported product structures characterizing the insertion of 8-oxodGTP across from C displayed a high B-factor (65.4 Å^2) for the inserted 8-oxoG(*anti*) and a loss of Watson–Crick base pairing interaction at the newly generated primer terminus post-catalysis. This is also in contrast to recent structures of pol β with terminal mispairs, which indicate that the mismatched termini adopt various distorted conformations (26). Ternary ground state structures, with 8-oxoG:C at the primer terminus and an incoming dCTP, show a clash between O8 and a non-bridging oxygen of the phosphate backbone that promotes a shift of the DNA backbone towards the protein active site. This shift is accommodated by a rotation of Arg254, which prevents the formation of a salt bridge between Arg254 and Asp256 (Figure 4C). Time lapse X-ray crystallography established that in order for catalysis to occur, Arg254 shifts back into position to coordinate Asp256. The observed requirement for this structural rearrangement is in agreement with the kinetics that show a substantially decreased catalytic efficiency with 8-oxoG:C at the primer terminus (Figure 1).

The clash between O8 and the phosphate backbone is also observed when 8-oxoG is in alternative registries. When 8-oxoG*(anti)* is in the template position with an incoming dCTP, the phosphodiester backbone shifts 3 Å away from O8. This shift is accommodated by the flexibility of the DNA at the bend in the templating strand, and does not alter any active site residues or alter the catalytic efficiency. The 8-oxoG:C base pair at the template n-1 position also maintains its catalytic efficiency; however, it does not require adjustment of the phosphodiester backbone (19). In the case of 8-oxodGTP insertion across from C, the clash between O8 and the oxygens of Pα are accommodated by an additional divalent metal cation during non-mutagenic insertion. Overall, it appears the templating strand can more effectively accommodate 8-oxoG(*anti*) than either the primer terminus or when the damage is the incoming nucleotide. This is reflective of the templating strand being more solvent exposed and therefore superiorly positioned to accommodate the clash between O8 and the non-bridging oxygens of the phosphate.

The Asp256 and Arg254 salt bridge serves an important role during catalysis

The nucleotidyl-transfer reaction is initiated by deprotonation of the primer DNA strand 3′-OH. The catalytic Mg^{2+} facilitates deprotonation by lowering the pK_a of the hydroxyl group and stabilizing the negative charge of the nucleophilic oxygen that attacks the phosphate of the incoming nucleotide. The nature of the 3′-OH proton acceptor is
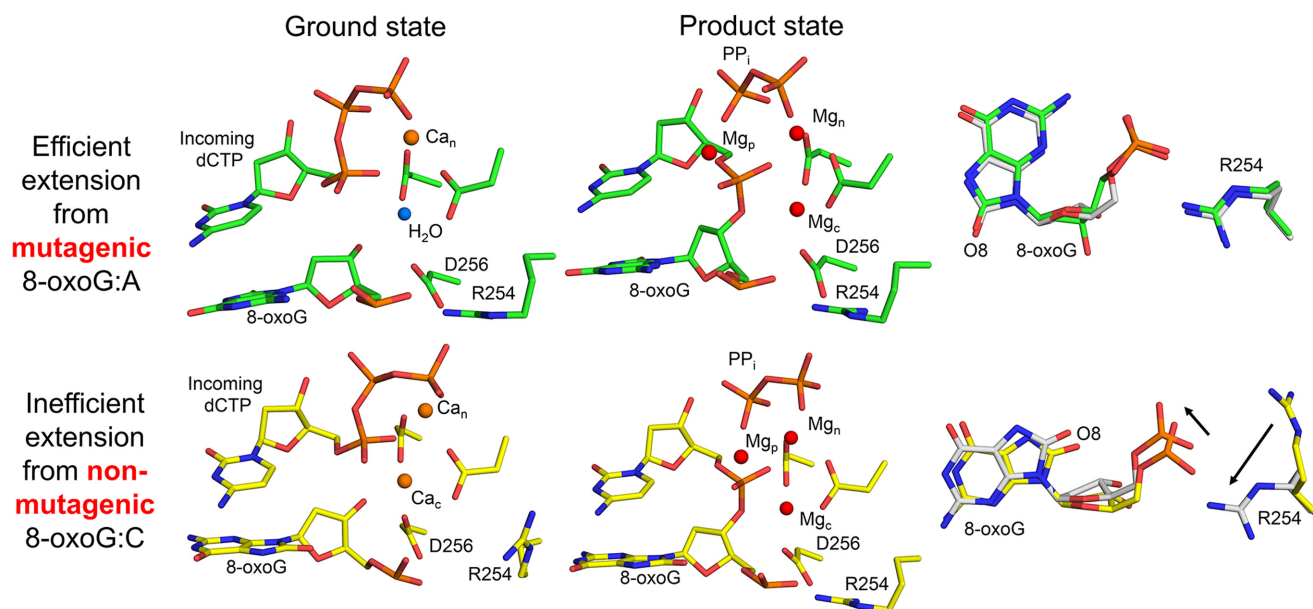
Figure 7. Overview comparing the structural changes observed during efficient, mutagenic extension from 8-oxodG:A (green) and inefficient, non-mutagenic extension from 8oxodG:C (yellow) terminal pairs. The right panels show overlays of the ground (colored) and product (gray) states.

an ongoing debate with two main theories for pol β (27,33–35). One theory is that the proton acceptor is a hydroxide anion in bulk water via a specific base mechanism. The second theory is that the proton acceptor is an active site group via a general base mechanism. In the former case, the proton transfer can be described by a pH dependent equilibrium between the protonated and deprotonated O3′, where the activated species forms a covalent bond with Pα of the dNTP and thus extends the primer DNA stand by one nucleotide. In the latter case, the pK_a values of both the donor (primer O3′) and the acceptor group (Asp256) are modulated by the catalytic Mg^{2+}. This results in the proton being transferred to the active site aspartic acid residue (Asp256) prior to it being transferred to bulk solvent.

The experimental data presented here supports a role for the carboxylate group of Asp256 in the deprotonation of the 3′-OH during catalysis, and suggests a key stabilizing role for Arg254. This is in agreement with quantum mechanical/molecular mechanical calculations indicating that the O3′ proton transfers to the OD2 oxygen of Asp256, which serves as a general base upon activation (35). Additionally, these computational studies suggested the critical role of Asp256 (OD2) is facilitated by a stabilizing salt bridge interaction between Asp256 (OD1) and the nearby Arg254. This is consistent with an experimental study that showed mutation of the homologous Arg254 residue in rat pol β to Ala decreases the k_{cat} from 51 to 1 min^{-1} (36). In a mutant of human pol β (D256E), a water molecule replaces OD2 of Asp256 and coordinates the catalytic metal (27). In contrast to the wild-type scenario, quantum calculations show this water is not involved in charge transfer to the catalytic metal. Additionally, the D256E pol β variant exhibited a three order of magnitude decrease in activity, and the structure demonstrates Arg254 repositions into a conformation where it does not interact with D256E (27).

Thus, Arg254 appears to play a critical role in positioning and stabilizing the carboxylate of Asp256. Our experiments also perturbed the nucleotidyl transfer reaction, but by altering the DNA substrate as opposed to using a variant enzyme. Experimental data presented here, and previously reported by others, suggests Asp256 is likely the proton acceptor in the nucleotidyl transferase reaction by pol β with Arg254 playing a key role in stabilizing Asp256 through a salt bridge interaction.

Broader implications for 8-oxoG at primer termini

It was unexpected for the extension from the mutagenic base to be favored, as it potentially augments the ability of the lesion to become hidden within the genome in its mutagenic form. Alternatively, in the case of 8-oxoG:C, rearrangements of key residues slow down catalysis and the polymerase 'pauses' on the DNA. This could potentially serve as a signal to other repair enzymes. The insertion of 8-oxoG opposite C, which would occur directly prior to the extension, is also catalytically unfavored relative to A. This would further delay the polymerase on the DNA in response to the lesion. Similarly, this contrast between mutagenic and non-mutagenic extension was observed during extended soaks in which 8-oxoG:C, but not 8-oxoG:A, at the primer terminus results in the reopening of the enzyme post-catalysis. This is in contrast to the correct insertion of a dNTP with a non-damaged primer terminus where pol β remains in the closed conformation upon extended soaks (18). 8-oxoG:C at the primer terminus promotes instability by exposing the cytotoxic nicked DNA repair intermediate, similarly to the insertion of 8-oxodGTP or incorrect insertion (4,18). Together, these results indicate the mutagenic 8-oxoG:A base pair is catalytically favored during DNA replication and re-

pair, underscoring the danger this common oxidative lesion poses to genome stability.

While the results presented here utilized pol β and a 1-nt gapped DNA substrate, the contacts and active site changes are likely applicable to other DNA polymerases. This is because the changes observed during extension from 8-oxoG are DNA centric, arising from the clash between O8 and the phosphate backbone, which would need accommodation by any polymerase's active site. The backbone Pα and 3′-OH move together and mediate the catalytic efficiency through altering the turnover rate. A phylogenetic analysis of DNA polymerase X-family members, of which pol β is a member, shows active site residues are conserved among many members. Specifically, Asp256 is highly conserved among X-family members (37). In pol λ, salt bridges between Arg488 (Arg254 in pol β) and Asp490 (Asp256 in pol β) are observed in the X-ray structures with an average distance of 2.8 Å. Therefore, it is likely that Arg488 plays an analogous stabilizing role in the nucleotidyl transfer reactions of pol λ, as proposed based on *ab initio* quantum mechanical/molecular mechanical methods (35,38). By performing MSA for the three X-family closed ternary complexes pol β (PDB 2FMS), pol λ (PDB 2PFO), and pol μ (PDB 2IHM) it was shown that two arginine residues likely contribute to substantial stabilization of the active site: Arg254 and Arg183 (pol β), Arg488 and Arg420 (pol λ) and Arg418 and Arg323 (pol μ). Therefore, the shift in the phosphate backbone arising from O8 will likely alter these X-family polymerases during DNA replication and repair. It remains to be elucidated how 8-oxoG at the primer termini is handled by other polymerase families (A, B and Y).

Outside of this study, the ability of polymerases to extend from DNA damage and the consequences of this extension have not been assiduously investigated. However, 8-oxoG regulation of telomerase activity was recently examined. In this study, it was uncovered that 8-oxodGTP insertion by telomerase terminates the chain, thereby preventing telomere restoration and promoting cell death (39). As the effects of 8-oxoG on the primer terminus presented here are DNA centric, it is likely that the clash observed between O8 and Pα in the 8-oxoG:C structures also occurs in the telomerase active site. The chain termination by 8-oxoG in telomerase could potentially be the result of an analogous clash, which alters key active site residues, thus providing a possible explanation for the fascinating result.

ACCESSION NUMBERS

Atomic coordinates and structure factors for the reported crystal structures have been deposited with the Protein Data bank under accession numbers 5V1G, 5V1F, 5V1P, 5V1R, 5V1I, 5V1J, 5V1H, 5V1N, 5V1O, and 5VEZ.

SUPPLEMENTARY DATA

Supplementary Data are available at NAR online.

FUNDING

Conflict of interest statement. None declared.

REFERENCES

1. Ames,B.N. and Gold,L.S. (1991) Endogenous mutagens and the causes of aging and cancer. *Mutat. Res.*, **250**, 3–16.
2. Topal,M.D. and Baker,M.S. (1982) DNA precursor pool: a significant target for N-methyl-N-nitrosourea in C3H/10T1/2 clone 8 cells. *Proc. Natl. Acad. Sci. U.S.A.*, **79**, 2211–2215.
3. Kamiya,H. and Kasai,H. (1995) Formation of 2-hydroxydeoxyadenosine triphosphate, an oxidatively damaged nucleotide, and its incorporation by DNA polymerases. Steady-state kinetics of the incorporation. *J. Biol. Chem.*, **270**, 19446–19450.
4. Freudenthal,B.D., Beard,W.A., Perera,L., Shock,D.D., Kim,T., Schlick,T. and Wilson,S.H. (2015) Uncovering the polymerase-induced cytotoxicity of an oxidized nucleotide. *Nature*, **517**, 635–639.
5. Tsuzuki,T., Egashira,A., Igarashi,H., Iwakuma,T., Nakatsuru,Y., Tominaga,Y., Kawate,H., Nakao,K., Nakamura,K., Ide,F. *et al.* (2001) Spontaneous tumorigenesis in mice defective in the MTH1 gene encoding 8-oxo-dGTPase. *Proc. Natl. Acad. Sci. U.S.A.*, **98**, 11456–11461.
6. Caglayan,M., Horton,J.K., Dai,D.P., Stefanick,D.F. and Wilson,S.H. (2017) Oxidized nucleotide insertion by pol beta confounds ligation during base excision repair. *Nat. Commun.*, **8**, 14045.
7. Hsu,G.W., Ober,M., Carell,T. and Beese,L.S. (2004) Error-prone replication of oxidatively damaged DNA by a high-fidelity DNA polymerase. *Nature*, **431**, 217–221.
8. Sakumi,K., Furuichi,M., Tsuzuki,T., Kakuma,T., Kawabata,S., Maki,H. and Sekiguchi,M. (1993) Cloning and expression of cDNA for a human enzyme that hydrolyzes 8-oxo-dGTP, a mutagenic substrate for DNA synthesis. *J. Biol. Chem.*, **268**, 23524–23530.
9. Gad,H., Koolmeister,T., Jemth,A.S., Eshtad,S., Jacques,S.A., Strom,C.E., Svensson,L.M., Schultz,N., Lundback,T., Einarsdottir,B.O. *et al.* (2014) MTH1 inhibition eradicates cancer by preventing sanitation of the dNTP pool. *Nature*, **508**, 215–221.
10. Huber,K.V., Salah,E., Radic,B., Gridling,M., Elkins,J.M., Stukalov,A., Jemth,A.S., Gokturk,C., Sanjiv,K., Stromberg,K. *et al.* (2014) Stereospecific targeting of MTH1 by (S)-crizotinib as an anticancer strategy. *Nature*, **508**, 222–227.
11. De Bont,R. and van Larebeke,N. (2004) Endogenous DNA damage in humans: a review of quantitative data. *Mutagenesis*, **19**, 169–185.
12. Fraga,C.G., Shigenaga,M.K., Park,J.W., Degan,P. and Ames,B.N. (1990) Oxidative damage to DNA during aging: 8-hydroxy-2′-deoxyguanosine in rat organ DNA and urine. *Proc. Natl. Acad. Sci. U.S.A.*, **87**, 4533–4537.
13. Culp,S.J., Cho,B.P., Kadlubar,F.F. and Evans,F.E. (1989) Structural and conformational analyses of 8-hydroxy-2′-deoxyguanosine. *Chem. Res. Toxicol.*, **2**, 416–422.
14. Oda,Y., Uesugi,S., Ikehara,M., Nishimura,S., Kawase,Y., Ishikawa,H., Inoue,H. and Ohtsuka,E. (1991) NMR studies of a DNA containing 8-hydroxydeoxyguanosine. *Nucleic Acids Res.*, **19**, 1407–1412.
15. Grollman,A.P. and Moriya,M. (1993) Mutagenesis by 8-oxoguanine: an enemy within. *Trends Genet.*, **9**, 246–249.
16. Beard,W.A. and Wilson,S.H. (2014) Structure and mechanism of DNA polymerase beta. *Biochemistry*, **53**, 2768–2780.
17. Freudenthal,B.D., Beard,W.A. and Wilson,S.H. (2015) New structural snapshots provide molecular insights into the mechanism of high fidelity DNA synthesis. *DNA Repair (Amst.)*, **32**, 3–9.
18. Freudenthal,B.D., Beard,W.A., Shock,D.D. and Wilson,S.H. (2013) Observing a DNA polymerase choose right from wrong. *Cell*, **154**, 157–168.
19. Batra,V.K., Shock,D.D., Beard,W.A., McKenna,C.E. and Wilson,S.H. (2012) Binary complex crystal structure of DNA polymerase beta reveals multiple conformations of the templating 8-oxoguanine lesion. *Proc. Natl. Acad. Sci. U.S.A.*, **109**, 113–118.
20. Beard,W.A. and Wilson,S.H. (1995) Purification and domain-mapping of mammalian DNA polymerase beta. *Methods Enzymol.*, **262**, 98–107.

21. Batra,V.K., Beard,W.A., Shock,D.D., Krahn,J.M., Pedersen,L.C. and Wilson,S.H. (2006) Magnesium-induced assembly of a complete DNA polymerase catalytic complex. *Structure*, **14**, 757–766.

22. Otwinowski,Z. and Minor,W. (1997) Processing of X-ray diffraction data collected in oscillation mode. *Macromol. Crystallogr. A*, **276**, 307–326.

23. Adams,P.D., Afonine,P.V., Bunkoczi,G., Chen,V.B., Davis,I.W., Echols,N., Headd,J.J., Hung,L.W., Kapral,G.J., Grosse-Kunstleve,R.W. *et al.* (2010) PHENIX: a comprehensive Python-based system for macromolecular structure solution. *Acta Crystallogr. D Biol. Crystallogr.*, **66**, 213–221.

24. Emsley,P. and Cowtan,K. (2004) Coot: model-building tools for molecular graphics. *Acta Crystallogr. D Biol Crystallogr.*, **60**, 2126–2132.

25. Beard,W.A., Shock,D.D. and Wilson,S.H. (2004) Influence of DNA structure on DNA polymerase beta active site function: extension of mutagenic DNA intermediates. *J. Biol. Chem.*, **279**, 31921–31929.

26. Batra,V.K., Beard,W.A., Pedersen,L.C. and Wilson,S.H. (2016) Structures of DNA polymerase mispaired DNA termini transitioning to pre-catalytic complexes support an induced-fit fidelity mechanism. *Structure*, **24**, 1863–1875.

27. Batra,V.K., Perera,L., Lin,P., Shock,D.D., Beard,W.A., Pedersen,L.C., Pedersen,L.G. and Wilson,S.H. (2013) Amino acid substitution in the active site of DNA polymerase beta explains the energy barrier of the nucleotidyl transfer reaction. *J. Am. Chem. Soc.*, **135**, 8078–8088.

28. Nakamura,T., Zhao,Y., Yamagata,Y., Hua,Y.J. and Yang,W. (2012) Watching DNA polymerase eta make a phosphodiester bond. *Nature*, **487**, 196–201.

29. Cavanaugh,N.A., Beard,W.A. and Wilson,S.H. (2010) DNA polymerase beta ribonucleotide discrimination: insertion, misinsertion, extension, and coding. *J. Biol. Chem.*, **285**, 24457–24465.

30. Jha,V. and Ling,H. (2017) Structural basis of accurate replication beyond a bulky major benzo[a]pyrene adduct by human DNA polymerase kappa. *DNA Repair (Amst.)*, **49**, 43–50.

31. Freudenthal,B.D., Beard,W.A. and Wilson,S.H. (2013) DNA polymerase minor groove interactions modulate mutagenic bypass of a templating 8-oxoguanine lesion. *Nucleic Acids Res.*, **41**, 1848–1858.

32. Vyas,R., Reed,A.J., Tokarsky,E.J. and Suo,Z. (2015) Viewing Human DNA polymerase beta faithfully and unfaithfully bypass an oxidative lesion by time-dependent crystallography. *J. Am. Chem. Soc.*, **137**, 5225–5230.

33. Klvana,M., Bren,U. and Florian,J. (2016) Uniform free-energy profiles of the P-O bond formation and cleavage reactions catalyzed by DNA polymerases beta and lambda. *J. Phys. Chem. B*, **120**, 13017–13030.

34. Matute,R.A., Yoon,H. and Warshel,A. (2016) Exploring the mechanism of DNA polymerases by analyzing the effect of mutations of active site acidic groups in Polymerase beta. *Proteins*, **84**, 1644–1657.

35. Lin,P., Pedersen,L.C., Batra,V.K., Beard,W.A., Wilson,S.H. and Pedersen,L.G. (2006) Energy analysis of chemistry for correct insertion by DNA polymerase beta. *Proc. Natl. Acad. Sci. U.S.A.*, **103**, 13294–13299.

36. Menge,K.L., Hostomsky,Z., Nodes,B.R., Hudson,G.O., Rahmati,S., Moomaw,E.W., Almassy,R.J. and Hostomska,Z. (1995) Structure-function analysis of the mammalian DNA polymerase beta active site: role of aspartic acid 256, arginine 254, and arginine 258 in nucleotidyl transfer. *Biochemistry*, **34**, 15934–15942.

37. Bienstock,R.J., Beard,W.A. and Wilson,S.H. (2014) Phylogenetic analysis and evolutionary origins of DNA polymerase X-family members. *DNA Repair (Amst.)*, **22**, 77–88.

38. Cisneros,G.A., Perera,L., Garcia-Diaz,M., Bebenek,K., Kunkel,T.A. and Pedersen,L.G. (2008) Catalytic mechanism of human DNA polymerase lambda with Mg2+ and Mn2+ from ab initio quantum mechanical/molecular mechanical studies. *DNA Repair (Amst.)*, **7**, 1824–1834.

39. Fouquerel,E., Lormand,J., Bose,A., Lee,H.T., Kim,G.S., Li,J., Sobol,R.W., Freudenthal,B.D., Myong,S. and Opresko,P.L. (2016) Oxidative guanine base damage regulates human telomerase activity. *Nat. Struct. Mol. Biol.*, **23**, 1092–1100.